Published in final edited form as:
Hear Res. 2010 May ; 263(1-2): 16–25. doi:10.1016/j.heares.2009.11.014.

Middle-Ear Pressure Gain and Cochlear Partition Differential Pressure in Chinchilla

Michael E. Ravicz[a,b,*], **Michaël C.C. Slama**[a,c], and **John J. Rosowski**[a,b,c]

[a]Eaton-Peabody Laboratory, Dept of Otolaryngology, Massachusetts Eye & Ear Infirmary, Boston MA 02114 USA

[b]Department of Otology and Laryngology, Harvard Medical School, Boston MA 02115 USA

[c]Harvard/MIT Division of Health Sciences and Technology, MIT, Cambridge, MA 02139 USA

Abstract

An important step to describe the effects of inner-ear impedance and pathologies on middle- and inner-ear mechanics is to quantify middle- and inner-ear function in the normal ear. We present middle-ear pressure gain $\mathbf{G_{MEP}}$ and trans-cochlear-partition differential sound pressure $\Delta\mathbf{P_{CP}}$ in chinchilla from 100 Hz to 30 kHz derived from measurements of intracochlear sound pressures in scala vestibuli $\mathbf{P_{SV}}$ and scala tympani $\mathbf{P_{ST}}$ and ear-canal sound pressure near the tympanic membrane $\mathbf{P_{TM}}$. These measurements span the chinchilla's auditory range. $\mathbf{G_{MEP}}$ had constant magnitude of about 20 dB between 300 Hz and 20 kHz and phase that implies a 40-μs delay, values with some similarities to previous measurements in chinchilla and other species. $\Delta\mathbf{P_{CP}}$ was similar to $\mathbf{G_{MEP}}$ below about 10 kHz and lower in magnitude at higher frequencies, decreasing to 0 dB at 20 kHz. The high-frequency rolloff correlates with the audiogram and supports the idea that middle-ear transmission limits high-frequency hearing, providing a stronger link between inner-ear macromechanics and hearing. We estimate the cochlear partition impedance $\mathbf{Z_{CP}}$ from these and previous data. The chinchilla may be a useful animal model for exploring the effects of nonacoustic inner-ear stimulation such as “bone conduction” on cochlear mechanics.

Keywords

Middle-ear sound transmission; introcochlear sound pressure; middle-ear gain; cochlear impedance; chinchilla

1. Introduction

The study of middle-ear and inner-ear mechanics explores the mechanisms by which sound pressure in the ear canal is converted to a stimulus for the sensory cells of the cochlea. With an understanding of these mechanisms comes an ability to describe the effects of middle-ear

*Corresponding author. Address: Eaton-Peabody Laboratory, Massachusetts Eye & Ear Infirmary, 243 Charles St., Boston MA 02114 USA. Tel.: +1 617 573-5591; FAX: +1 617 720-4408. Mike_Ravicz@meei.harvard.edu.

[3]$\mathbf{Z_{CP}}$ also includes the influence of the helicotrema, which is not explicitly included in the model but has been postulated to affect $\mathbf{Z_{CP}}$ at very low frequencies (Dallos, 1970).

and inner-ear pathologies on hearing, to develop more reliable methods to diagnose pathologies, and to evaluate the mechanisms by which those pathologies affect hearing.

Middle-ear and inner-ear pathologies affect hearing by modifying the effective input to the cochlea. It has been proposed (e.g., Dallos, 1970) that the effective cochlear input is the differential sound pressure across the cochlear partition: the difference between scala vestibuli sound pressure $\mathbf{P_{SV}}$ and scala tympani sound pressure $\mathbf{P_{ST}}$. ($\mathbf{P_{SV}}$, $\mathbf{P_{ST}}$, and all other quantities shown in bold face are complex variables with magnitude and phase that are functions of frequency *f*.) This differential sound pressure $\mathbf{P_{SV}} - \mathbf{P_{ST}}$ induces motion of the cochlear partition that stimulates the sensory cells of the organ of Corti and leads to hearing perception. Comparisons of differential sound pressure to measures of organ of Corti sensory cell activity (cochlear potential CP – Nedzelnisky, 1980; Dancer and Franke, 1980) and analysis of hearing in patients in whom the ossicular chain is missing (Peake et al., 1992) provide support for this assertion.

In the past, researchers have used measurements at more peripheral points, such as tympanic membrane (TM) admittance, umbo or stapes velocity, and/or models of middle-ear and cochlear function based on anatomy and material properties to estimate the effective cochlear input, establish the relationship between cochlear input and ear-canal sound pressure or auditory threshold, and gauge the effects of middle-ear pathologies or reconstructions on cochlear function and hearing. Measuring sound pressures inside the cochlea has two primary advantages over more peripheral measurements: (1) These sound pressures within the cochlear scalae are the pressures actually applied to the cochlea, so complications such as which of the multiple modes of stapes motion produce effective cochlear input are moot; and (2) since sound pressure is a scalar quantity, the sound pressure at a given location inside the cochlea (unlike stapes velocity) is independent of the measurement direction.

In this paper we present new measurements of $\mathbf{P_{SV}}$ and $\mathbf{P_{ST}}$ in chinchilla using miniature fiber-optic pressure sensors (Olson, 1998; Slama, 2008; Slama et al., 2009, in press). These measurements are used with measurements of ear-canal sound pressure near the tympanic membrane $\mathbf{P_{TM}}$ to compute the middle-ear pressure gain $\mathbf{G_{MEP}}$ and the normalized differential trans-cochlear-partition pressure $\Delta\mathbf{P_{CP}}$:

$$\mathbf{G_{MEP}} = \mathbf{P_{SV}} / \mathbf{P_{TM}}; \text{and} \tag{1a}$$

$$\Delta\mathbf{P_{CP}} = (\mathbf{P_{SV}} - \mathbf{P_{ST}}) / \mathbf{P_{TM}} = \mathbf{G_{MEP}} - \mathbf{P_{STn}}, \tag{1b}$$

where $\mathbf{P_{STn}} = \mathbf{P_{ST}}/\mathbf{P_{TM}}$. $\Delta\mathbf{P_{CP}}$ represents the effective input to the cochlear partition for a given sound pressure in the ear canal, as mentioned above. We use $\mathbf{G_{MEP}}$ and $\Delta\mathbf{P_{CP}}$ to compute the input impedance of the cochlear partition $\mathbf{Z_{CP}}$ from previous measurements of the cochlear input impedance (Slama, 2008; Slama et al., in press).

The middle-ear pressure gain is one part of the description of the transformation of sound from the ear canal to the cochlea by the middle ear (the ratio of stapes velocity to $\mathbf{P_{TM}}$ is the other, e.g., Shera and Zweig, 1992). These new measurements of $\mathbf{P_{SV}}$ and $\mathbf{P_{ST}}$, though somewhat preliminary, extend recent measurements of $\mathbf{G_{MEP}}$ in chinchilla in our laboratory (Slama, 2008; Slama et al., 2009) to higher frequencies, add to a small but growing database of cochlear sound pressure transfer functions in normal ears in various species, and therefore represent a step toward a more complete understanding of middle-ear sound transmission.

2. Methods

2.1 Preparation

These experiments were performed in accordance with guidelines published by the U.S. Public Health Service and were approved by the Massachusetts Eye & Ear Infirmary Institutional Animal Care and Use Committee. Five ears in four chinchillas were used in this study. (Several other ears were used in preliminary experiments or had various mishaps.) Animals remained alive throughout the experiment. Most of the preparation has been described in detail previously (Songer and Rosowski, 2006). Briefly, each animal was anesthetized with Nembutal (50 mg/kg) and Ketamine (40 mg/kg) and tracheotomized, the external ear was removed (usually the left), skin and soft tissue were removed from the skull around the bony external ear canal, and openings were made in the bulla wall superior and posterior to the ear canal. Lidocaine (1%) was sometimes used as a topical anesthetic in sensitive areas. Through the superior opening, the tendon of the tensor tympani muscle and the tympanic branch of the facial nerve (which innervates the stapedius muscle) were cut to prevent random contractions of these muscles during the experiment from affecting results (see Rosowski et al., 2006).

A short brass tube was glued to the skull around the bony ear canal to allow a sound source to be coupled repeatably to the ear. A stainless steel sleeve was glued under the brass coupler to allow a probe tube microphone tip to measure sound pressure $\mathbf{P_{TM}}$ within 1–1.5 mm of the umbo within the tympanic membrane (TM) – see Figure 1. A thin web of bone that obscures the view of the stapes and the oval-window (OW) and round-window (RW) niches was carefully chipped away to provide access to the bone of the vestibule just posterior to the oval window and to the surface of the cochlear capsule inferior and posterior to the round window. A small hole was drilled through the vestibular wall with a fine pick to allow a pressure sensor to measure sound pressure within scala vestibuli $\mathbf{P_{SV}}$. The desired hole size was between 150 and 200 μm diameter, slightly larger than the sensor tip (145 μm diameter), but in two of the ears the hole size was closer to 400 μm dia., and in two ears the bone between the hole and the OW cracked. (The cracked bone was not displaced.) The effect of the crack is discussed later.

After $\mathbf{P_{SV}}$ measurements, a similar small hole was made in the cochlear capsule approximately 1 mm inferior to the RW (near the apical extent of the “hook” region) with a 0.006” (150 μm) pivot drill. The more exposed location on the cochlear capsule allowed the drill to be brought perpendicular to the surface of the cochlear capsule and allowed visibility of the tip. With this drill, a hole could be made through the hard bone of the cochlear capsule into scala tympani for $\mathbf{P_{ST}}$ measurements fairly quickly, and hole size could be controlled closely. The tight quarters and poor visibility in the OW niche and the non-perpendicularity of the vestibular wall relative to the access direction precluded using the drill for the scala vestibuli hole.

2.2 Stimuli, responses, and equipment

Stimuli were synthesized by computer and/or played by a computer-controlled signal generator (Hewlett-Packard 33120A). Stimulus levels were set by programmable attenuators (Tucker-Davis PA-5) and a reconstruction filter with programmable gain (Krohn-Hite 3901). A power amplifier (Crest 1001A) was used to drive a low-impedance earphone (Radio Shack 40-1377) to generate sound in the ear canal or a shaker for pressure sensor calibration. Two types of sound stimuli were used: A broadband chirp with uniform component magnitude from 49 Hz to 49 kHz, or a sequence of tones. Two sequences were used: 98 Hz – 49 kHz at 6 pts/octave (as permitted by a 49-Hz frequency spacing) and 14 – 49 kHz at 12 pts/octave. Chirps allowed overview measurements to be made quickly, provided sufficient frequency resolution to guide $\mathbf{P_{SV}}$ and $\mathbf{P_{ST}}$ phase unwrapping at high frequencies, and were useful for checking that measurements were stable. Tone sequences had better signal-to-noise ratio and allowed higher stimulus levels to be used at high frequencies if necessary.

Three types of responses were measured: (1) sound pressure (air) near the TM ($\mathbf{P_{TM}}$), also in the ear canal near the acoustic source ($\mathbf{P_{EC}}$) as a check; (2) sound pressure (liquid) in scala vestibuli ($\mathbf{P_{SV}}$) and in scala tympani ($\mathbf{P_{ST}}$); and (3) cochlear potential (CP) near the RW. Ear canal sound pressure was measured with small microphones ($\mathbf{P_{EC}}$: Knowles EK-3027; $\mathbf{P_{TM}}$: Knowles FG23652) attached to thin probe tubes. Scalae sound pressures were measured with fiber-optic pressure sensors (Olson, 1998) inserted 150–500 μm into the scalae holes described above. CP was measured with a ball electrode on the cochlear capsule ~1 mm inferior to the RW. Responses were amplified (air sound pressure and CP: Grass P5; scalae sound pressure: custom differential amplifiers), digitized at 226 kHz by a data acquisition board (National Instruments 4451), and saved on a computer. Two response channels could be saved at a time.

2.3 Microphone and sensor calibration

Microphones were calibrated against a 1/4" reference microphone (Larson-Davis 2530) at low frequencies and against a 1/8" reference microphone (G.R.A.S. 40DP) at high frequencies (e.g., Ravicz et al., 2007), using a broadband chirp stimulus. Microphones were calibrated at the beginning and end of each experiment.

The calibration of the pressure sensors includes two components: the frequency response and the sensitivity. For these sensors, the frequency response is nearly constant: the magnitude and phase of the ratio of output voltage $\mathbf{v_{sens}}(f)$ to sound pressure $\mathbf{P_0}(f)$ decrease smoothly and only slightly (2–10 dB and 0.1 cycle) between 100 Hz and 50 kHz (see also Olson, 1998), and this frequency shape remains constant until the sensor fails. In contrast, the sensitivity (typical $|v_{sens} / P_0|$ across frequency) can be quite variable, and this variability in sensitivity affects all frequencies equally (Olson, 1998). We therefore used two methods to calibrate the sensors: in air, which gave a more accurate frequency response but a variable estimate of sensitivity (and some sensors were insensitive in air); and in water, which gave a more reliable estimate of sensitivity *in vivo* and was quicker and easier to perform during experiments but was less accurate at high frequencies.

For air calibration, the tip of the pressure sensor was positioned within 1 mm of the 1/8" reference microphone (see Ravicz et al., 2007), and sensor output was measured in response to a tone sequence or broadband chirp. For water calibration, the sensor tip was submerged 1 mm deep into a small vial attached to a shaker head and accelerometer (Brüel+Kjær 4290 – see Olson, 1998). Acceleration of the vial in response to a tone stimulus generated a sound pressure in the vial (e.g., Schloss and Strasberg, 1962). Water calibrations were generally more repeatable than air calibrations, especially at low frequencies; but water calibrations were sometimes spuriously high at high frequencies (due to a low signal-to-noise ratio, sensitivity to bubbles in the vial, and/or uncertainty in high-frequency acceleration due to a shaker resonance not far above the highest frequency measured). We used water calibrations at frequencies where they were not affected by the factors above and (for some ears) used smoothed air calibrations at high frequencies.

Some investigators in our laboratory (Slama, 2008; Slama et al., in press) have the monitored sensor DC output voltage (which depends on the amount of light reflected from the sensor diaphragm) as an indicator that the sensor sensitivity *in vivo* is the same as during calibration. We did not use stable DC as a criterion.

2.4 Experimental procedure

Experiments proceeded as follows: After the ear canal coupler was placed and after holes were made into the middle ear but before the bone web near the facial nerve was removed, CP and ear canal sound pressures $\mathbf{P_{EC}}$ and $\mathbf{P_{TM}}$ were measured at several stimulus levels with chirp stimuli. CP was measured again after the bone web was removed and once again after the scala

vestibuli hole was drilled. The CP showed a compressive nonlinearity with stimulus level and decreased less than 20 dB after these manipulations, which confirmed that the ossicular chain was intact and the cochlea was healthy.[1]

After calibration, a pressure sensor was inserted 150–500 μm deep into the scala vestibuli hole. $\mathbf{P_{SV}}$ was measured at several stimulus levels with chirps and with tone sequences. $\mathbf{P_{TM}}$ was measured simultaneously, including at lower stimulus levels to preclude distortion from driving the microphones too hard. Following these first $\mathbf{P_{SV}}$ measurements, the pressure sensor was withdrawn and recalibrated; then it was reinserted into scala vestibuli for another measurement series and withdrawn again for another calibration. At this point the hole was drilled into scala tympani, and another pressure sensor was calibrated and inserted 150–300 μm deep into this hole (but still far from the organ of Corti). $\mathbf{P_{ST}}$ was measured simultaneously with $\mathbf{P_{TM}}$ as described above or simultaneously with $\mathbf{P_{SV}}$. In some ears, $\mathbf{P_{SV}}$ measurements were repeated at different insertion depths. Sensor outputs were within 2–3 dB of maximal for insertion depths of at least 150 μm. At least two measurement series were performed, and both sensors were removed and recalibrated after each series. $\mathbf{P_{SV}}$ and $\mathbf{P_{ST}}$ measurements generally varied by less than 2–3 dB between series.

At this point, the ossicular chain was disrupted, and $\mathbf{P_{SV}}$, $\mathbf{P_{ST}}$, and $\mathbf{P_{TM}}$ were measured as described above. Following these measurements, the experiment was terminated by an overdose of anesthesia and all sensors and microphones were recalibrated. For all data shown in this paper, sensor calibrations were constant within 2 dB throughout the measurements.

3. Results

To allow comparisons with other measurements taken at different stimulus levels or in different ears, all $\mathbf{P_{SV}}$ and $\mathbf{P_{ST}}$ data presented here are normalized by $\mathbf{P_{TM}}$. The ratio of $\mathbf{P_{SV}}$ to $\mathbf{P_{TM}}$ is the middle-ear pressure gain $\mathbf{G_{MEP}}$. Normalized $\mathbf{P_{ST}}$ is denoted as $\mathbf{P_{STn}}$. In all figures, data have been omitted at frequencies above 25–30 kHz where the accuracy of $\mathbf{P_{TM}}$ measurements was suspect.

3.1 Middle-ear pressure gain

The middle-ear pressure gain $\mathbf{G_{MEP}}$ was measured in five ears and is shown in Figure 2. The measurement location was at the very base of the cochlea, which presumably corresponds to a best frequency of 22 kHz (by the cochlear map of Eldridge et al., 1981). In the two ears in which the bone near the oval window was cracked (ch06R, ch07L), $\mathbf{G_{MEP}}$ is different than in the other three ears below 1 kHz (described further below), but above 1 kHz $\mathbf{G_{MEP}}$ is similar among all ears.

At the lowest frequencies measured (100–250 Hz) $|\mathbf{G_{MEP}}|$ increased with frequency and $\angle\mathbf{G_{MEP}}$ is near +0.25 cycles in the three ears with no OW crack (solid gray lines), which is consistent with the stiffness dominance of the middle ear at these low frequencies (e.g., Rosowski et al., 2006). A small mass component to inner-ear dynamics could also contribute to this low-frequency increase. Above a magnitude peak at 250 Hz (1 kHz in the OW-cracked ears), $|\mathbf{G_{MEP}}|$ was generally +15 to +27 dB in all ears up to ~20 kHz and $\angle\mathbf{G_{MEP}}$ was near 0 to about 8 kHz. There was a dip in $|\mathbf{G_{MEP}}|$ and a ripple in $\angle\mathbf{G_{MEP}}$ near 2.5 kHz, consistent with a resonance between the bulla holes and the air in the middle ear (Rosowski et al., 2006). Except for this dip, $|\mathbf{G_{MEP}}|$ was generally flat with frequency between the frequency where $\angle\mathbf{G_{MEP}} < 0.25$ cycles (0.25–1 kHz) and 15–20 kHz. This $|\mathbf{G_{MEP}}|$ flatness and

[1]The fluid environment around the RW electrode changed when the SV hole was drilled, so direct comparisons of CP level are misleading. In one ear (not used due to sensor problems), CP was measured after the ST hole was drilled, and CP levels and nonlinearities were unchanged.

$\angle \mathbf{G_{MEP}}$ near 0 are consistent with the cochlea being a resistance-dominated system over a large frequency range.

The gradual accumulation of $\angle \mathbf{G_{MEP}}$ to about 1 cycle at 25 kHz indicates a delay of about 40 μsec. This delay is consistent with that computed from the phase of the $\mathbf{P_{TM}}$-to-stapes velocity middle-ear transfer function measured by Songer and Rosowski (2006) and suggests that the delay is caused mostly by the middle ear.

In the two ears with the OW crack, the $|\mathbf{G_{MEP}}|$ peak and $\angle \mathbf{G_{MEP}}$ transition seen in the normal ears at about 250 Hz occurred at about 1 kHz, and $|\mathbf{G_{MEP}}|$ decreased rapidly as frequency decreased below 1 kHz. $\angle \mathbf{G_{MEP}}$ was near +0.25 cycles from the lowest frequency measured to about 1 kHz. The differences in $\mathbf{G_{MEP}}$ between these two ears and the rest are consistent with a mass in parallel with the cochlear resistance whose impedance is considerably less than the cochlear resistance at low frequencies. If this view is valid, then the effect of the crack near the OW is to relieve cochlear sound pressure at low frequencies and cause the middle-ear output to bypass the cochlea.

$|\mathbf{G_{MEP}}|$ remained in the +10 to +25 dB range up to approximately 20 kHz in all ears. Above 20–25 kHz $|\mathbf{G_{MEP}}|$ dropped precipitously to < 0 dB in all ears, and $\angle \mathbf{G_{MEP}}$ diverged among ears. $\mathbf{P_{SV}}$ measurements were generally 20–40 dB above the noise floor over most of the frequency range and at least 10 dB above the noise floor to about 40 kHz.

The logarithmic mean of $\mathbf{G_{MEP}}$ in all ears was computed and is shown as the solid black line. Data from the two ears with the OW crack were omitted from calculations of the mean at frequencies below 1 kHz.

3.2 Normalized scala tympani sound pressure

Scala tympani sound pressure $\mathbf{P_{STn}}$ (normalized by $\mathbf{P_{TM}}$) was measured in four of the five ears above and is shown in Figure 3. The best frequency corresponding to the measurement location (~1 mm from the RW) was, we believe, approximately 10–12 kHz (see Eldridge et al., 1981). As for $\mathbf{G_{MEP}}$ (described above), $\mathbf{P_{STn}}$ was different in the two ears with the OW crack (ch06R, ch07L - dashed gray lines) than in the other two ears (solid gray lines) below 1 kHz but was similar among all ears above 1 kHz. As above, the logarithmic mean of $\mathbf{P_{STn}}$ below 1 kHz in the two ears with no OW crack and in all ears at higher frequencies is shown by the solid black line.

In the two ears with no OW crack, $|\mathbf{P_{STn}}|$ was approximately −5 dB at frequencies below 500 Hz, and $\angle \mathbf{P_{STn}}$ was approximately 0 up to 5 kHz. In the two ears with the OW crack, $|\mathbf{P_{STn}}|$ was much lower (approximately −20 dB) at frequencies below 500 Hz, and $\angle \mathbf{P_{STn}}$ decreased gradually from nearly +0.5 cycles to 0 at 5 kHz. In these ears, $|\mathbf{P_{STn}}|$ is at the noise floor below 300 Hz. In all ears $|\mathbf{P_{STn}}|$ increased to about +20 dB near 8 kHz and then decreased to about +10 dB at 20 kHz. $\angle \mathbf{P_{STn}}$ accumulated as frequency increased above 5 kHz, to about −0.7 cycles by 20 kHz, which corresponds to a delay of about 35 μsec. $\mathbf{P_{STn}}$ shows a magnitude dip and phase ripple near 2.5 kHz similar to that seen in $\mathbf{G_{MEP}}$ in these ears (see previous section). Above 20–25 kHz $|\mathbf{P_{STn}}|$ dropped rapidly and $\angle \mathbf{P_{STn}}$ accumulated rapidly.

4. Discussion

4.1 Ratio of P_{ST} to P_{SV} and comparison to a simple cochlear model

Figure 4 shows the ratio of $\mathbf{P_{STn}}$ to $\mathbf{G_{MEP}}$ in each of the four ears of Figure 3. For measurements made with equal TM sound pressure, this ratio is equivalent to the ratio of $\mathbf{P_{ST}}$ to $\mathbf{P_{SV}}$ (e.g., for $\mathbf{P_{ST}}$ and $\mathbf{P_{SV}}$ measured simultaneously.) It is notable that $|\mathbf{P_{STn}}/\mathbf{G_{MEP}}|$ was similar in all ears, even those with an OW crack (dashed gray lines), which indicates that the OW crack

affected $\mathbf{P_{ST}}$ and $\mathbf{P_{SV}}$ equally and implies that the mechanical properties of the cochlear partition, which presumably influences the ratio of $\mathbf{P_{ST}}$ to $\mathbf{P_{SV}}$, were not altered by the OW crack.

At low frequencies, $|\mathbf{P_{STn}}/\mathbf{G_{MEP}}|$ was very small, consistend with $|\mathbf{G_{MEP}}| \gg |\mathbf{P_{STn}}|$ as described above. $|\mathbf{P_{STn}}/\mathbf{G_{MEP}}|$ increased with frequency and leveled off above about 5 kHz. The mean $|\mathbf{P_{STn}}/\mathbf{G_{MEP}}|$ was about −6 dB between 5 and 20 kHz, which implies that $|\mathbf{P_{STn}}| \approx |\mathbf{G_{MEP}}| / 2$.

Near 20 kHz, $|\mathbf{P_{STn}}|$ approached $|\mathbf{G_{MEP}}|$ (the mean $|\mathbf{P_{STn}}/\mathbf{G_{MEP}}|$ approached 0 dB), and at higher frequencies $|\mathbf{P_{STn}}/\mathbf{G_{MEP}}|$ was between −10 and 0 dB. $\angle(\mathbf{P_{STn}}/\mathbf{G_{MEP}})$ decreased slowly from about +0.2 cycles at 500 Hz to 0 at 20–25 kHz. This relationship between $\mathbf{P_{STn}}$ and $\mathbf{G_{MEP}}$ implies that the structure(s) that influences the relative values of $\mathbf{P_{ST}}$ and $\mathbf{P_{SV}}$ gradually decreases in importance as frequency increases. If this structure is the cochlear partition, this result implies that cochlear partition impedance influences $\mathbf{P_{ST}}$ at low frequencies but not at high. Above 25 kHz $\angle(\mathbf{P_{STn}}/\mathbf{G_{MEP}})$ decreased by one cycle.

The relationship between $\mathbf{G_{MEP}}$ and $\mathbf{P_{STn}}$ is consistent with a simple model of cochlear sound pressure (adapted and expanded from Olson, 2001) shown as an inset to Fig. 4 and described in more detail in the Appendix. Because $\mathbf{P_{SV}}$ and $\mathbf{P_{ST}}$ were measured at slightly different cochlear locations ($\mathbf{P_{SV}}$ at the base, and $\mathbf{P_{ST}}$ about 2 mm from the base; see Sec. 3.2), the scala fluid mass terms M_{SV} and M_{ST} include the mass of the fluid between the $\mathbf{P_{SV}}$ measurement location or the round window and the $\mathbf{P_{ST}}$ measurement locations. M_{ST} also includes the mass of the fluid between the $\mathbf{P_{ST}}$ sensor tip and the cochlear partition (see Olson, 2001). Because in our preparation the RW was kept intact, our model also includes a round window compliance C_{RW} (important at low frequencies).

The model prediction of $\mathbf{P_{ST}}/\mathbf{P_{SV}}$ (black dashed line) is a good match to both the magnitude and phase of the mean $\mathbf{P_{STn}}/\mathbf{G_{MEP}}$ across nearly the entire frequency range of measurement, which implies that the model probably provides a reasonable description of the relative sound pressures within the actual cochlea. The model suggests that:

(a) The impedance of the cochlear partition is the primary determinant of the ratio of $\mathbf{P_{ST}}$ to $\mathbf{P_{SV}}$ at frequencies below about 5 kHz. At higher frequencies, the mass of the SV fluid between the OW and the $\mathbf{P_{ST}}$ measurement location influences $\mathbf{P_{ST}}/\mathbf{P_{SV}}$.

(b) The impedance of the cochlear partition is determined primarily by the cochlear resistance below 20 kHz.

(c) At very low frequencies (below 300 Hz) the stiffness of the RW membrane influences $\mathbf{P_{ST}}/\mathbf{P_{SV}}$.

4.2 Differential trans-cochlear-partition pressure

The differential sound pressure across the cochlea partition $\Delta\mathbf{P}_{CP}$ computed from $\mathbf{P_{STn}}$ and $\mathbf{G_{MEP}}$ by Eq. 1b is shown for each of the four ears in Figure 5. $\Delta\mathbf{P}_{CP}$ had many of the same features as $\mathbf{G_{MEP}}$, which is not surprising given that $|\mathbf{G_{MEP}}| > |\mathbf{P_{STn}}|$ over most of the frequency range of measurements. At frequencies above a few kHz, $|\Delta\mathbf{p}_{CP}| < |\mathbf{G_{MEP}}|$, because $\mathbf{P_{STn}}$ (which is subtracted from $\mathbf{G_{MEP}}$) had the same phase and nearly the samemagnitude as $\mathbf{G_{MEP}}$ (see Fig. 4). At 20 kHz $|\Delta\mathbf{P_{CP}}| \approx 0$ dB and $\angle\Delta\mathbf{P_{CP}}$ accumulated >1 cycle. Above 25 kHz $|\Delta\mathbf{P_{CP}}|$ decreased rapidly and $\angle\Delta\mathbf{P_{CP}}$ accumulated an additional cycle.

4.3 Effects of experimental inner-ear modifications on G_{MEP}, P_{STn}, and ΔP_{CP}

All of our cochlear measurements involve inner-ear modifications, because holes must be made into the cochlear scalae to place the sensors. Preliminary data from such modifications suggest that their effects are small and limited in frequency range.

4.3.1 Effects of scala vestibuli hole—We did our best to keep the scala vestibuli and scala tympani holes as small as possible – just large enough for the sensor tip – but we were not always successful in early experiments. In those ears in which we cracked the bone around the OW (ch06R, ch07L), the low-frequency magnitude reduction and phase increase in $\mathbf{G_{MEP}}$ and $\mathbf{P}_{STn}$ (Figs. 2 and 3) are consistent with the low impedance of a large hole shunting the large cochlear resistance. The similarity in effects (Fig. 4) suggests that at low frequencies $\mathbf{P_{ST}}$ is determined primarily by $\mathbf{P_{SV}}$ and the properties of the cochlear partition rather than by input by any other path. Because $\Delta\mathbf{P_{CP}}$ is determined primarily by $\mathbf{G_{MEP}}$ at low frequencies (Figs. 4 and 5), the effect of the scala vestibuli hole on $\Delta\mathbf{P_{CP}}$ was similar to its effect on $\mathbf{G_{MEP}}$.

We did not attempt to seal the sensor in the scala vestibuli hole, but Slama (2008, Slama et al., in press) showed in one ear that sealing the sensor hole increased $|\mathbf{G_{MEP}}|$ by as much as 10 dB and reduced $\angle\mathbf{G_{MEP}}$ toward zero below 200 Hz, with only small effects at higher frequencies. Neither we nor Slama (2008) observed any consistent relationship between scala vestibuli hole size and low-frequency $\mathbf{G_{MEP}}$. We made no $\mathbf{P}_{ST}$ measurements before making the scala vestibuli hole, but $\mathbf{P}_{ST}$ was similar whether the scala vestibuli hole was filled by a sensor or left open.

Because the cracked OW bone had no consistent effect on $\mathbf{G_{MEP}}$ and $\mathbf{P}_{STn}$ at high frequencies (Figs. 2 and 3), we believe that the scala vestibuli hole had no significant effect on high-frequency $\Delta\mathbf{P_{CP}}$.

4.3.2 Effects of scala tympani hole—Opening a hole into scala tympani had a smaller and contrary effect on $\mathbf{G_{MEP}}$ than the scala vestibuli hole: a small (2–3 dB) increase in $|\mathbf{G_{MEP}}|$ and ~0.1-cycle decrease in $\angle\mathbf{G_{MEP}}$ below 1 kHz (data not shown). We had good success in keeping the scala tympani hole small, so that the sensor tip filled it. When the sensor was inserted into the scala tympani hole, $\mathbf{G_{MEP}}$ was similar to its value before scala tympani was opened.

4.4 Effects of experimental middle-ear modifications on $_{GMEP}$, P_{STn}, and ΔP_{CP}

We measured $\mathbf{G_{MEP}}$, $\mathbf{P}_{STn}$, and $\Delta\mathbf{P_{CP}}$ in two ears (ch07L, ch08L) after disrupting the ossicular chain (interrupting the incudostapedial joint, subluxing the stapes, and/or breaking the incus long process) to estimate the importance of sound energy delivered through the RW and the cochlear capsule on intracochlear sound pressures. We found that, with the ossicular chain disrupted, (a) $|\mathbf{G_{MEP}}|$ and $|\mathbf{P}_{STn}|$ never exceeded 0 dB (pressure gain was always <1) across the frequency range, except for a narrow band around 15 kHz. Both $|\mathbf{G_{MEP}}|$ and $|\mathbf{P}_{STn}|$ were substantially less than 0 dB (−20 to −30 dB) at frequencies above 3 kHz except as noted above. (b) $\angle\mathbf{G_{MEP}}$ decreased by 0.25 – 0.5 cycle between 500 Hz and about 10 kHz, though $\angle\mathbf{P_{STn}}$ did not change. $\angle\mathbf{G_{MEP}}$ and $\angle\mathbf{P_{STn}}$ accumulated faster above 15 kHz than in the undisrupted state. (c) $|\mathbf{P_{STn}}|$ was substantially greater than $|\mathbf{G_{MEP}}|$ above 4 kHz, so $\Delta\mathbf{P_{CP}} \approx \mathbf{G_{MEP}}$ below 1 kHz and $\Delta\mathbf{P_{CP}} \approx \mathbf{P_{STn}}$ above 4 kHz. (d) $|\mathbf{G_{MEP}}|$ and $\Delta\mathbf{P_{CP}}$ were reduced substantially at nearly all frequencies, which demonstrates that the ossicular chain is the primarily route of sound conduction to the cochlea at frequencies up to at least 30 kHz, a range that spans the chinchilla's range of hearing (Slama, 2008; Slama et al., in press).

4.5 Comparison of G_{MEP} with other studies

Middle-ear pressure gain in chinchilla has been measured in two other studies of which we are aware: by Slama (2008; Slama et al., 2009, in press), using the same technique in the same laboratory as this study, also using a fiber-optic pressure sensor; and by Décory (1989; Décory et al., 1990) using a piezoelectric hydrophone with a narrow probe tube inserted into a scala vestibuli hole of diameter similar to ours (but a different location – see below). $\mathbf{G_{MEP}}$ in these other studies is compared with our mean results in Figure 6.

$\mathbf{G_{MEP}}$ from all studies is fairly similar between 300 Hz and 5 kHz: all show $|\mathbf{G_{MEP}}|$ fairly flat with frequency and $\angle\mathbf{G_{MEP}}$ accumulating slowly. In all three studies, $|\mathbf{G_{MEP}}|$ decreased at lower frequencies and $\angle\mathbf{G_{MEP}}$ increased to about +0.25 cycles. The lower frequency of the flat $|\mathbf{G_{MEP}}|$ plateau varied among the studies: highest in Décory, lowest in Slama. As mentioned in Section 4.3 above, sealing the scala vestibuli hole moved this frequency down while a crack near the OW moved this frequency up, so hole sealing is a likely source of low-frequency $\mathbf{G_{MEP}}$ differences.

Another argument in support of a connection between the lower $|\mathbf{G_{MEP}}|$ plateau frequency and the sealing of the scala vestibuli hole is provided by comparing two measures of CP frequency dependence, magnitude across frequency (Drescher and Eldredge, 1974) and thresholds as a function of frequency (Dallos, 1970), with $|\mathbf{G_{MEP}}|$. It has been established (Dancer and Franke, 1980, in guinea pig) that CP varies with $|\Delta\mathbf{P_{CP}}|$, and at low frequencies $|\Delta\mathbf{P_{CP}}|$ and $|\mathbf{G_{MEP}}|$ are nearly identical (compare Figs. 2, 4, and 5), so the spectral shape of CP should be a good descriptor of the frequency dependence of $|\mathbf{G_{MEP}}|$ in the undisturbed inner ear. Both of these CP measurements show CP amplitude remaining nearly constant with frequency down to 100 Hz (the Dallos (1970) CP shows a decrease below 100 Hz), which implies that in the undisturbed inner ear the $|\mathbf{G_{MEP}}|$ plateau should extend to lower frequencies than this and previous studies have shown.

In the middle frequency range where $\mathbf{G_{MEP}}$ is approximately constant, $|\mathbf{G_{MEP}}|$ is generally about 10 dB lower in this study than in the others over this frequency range. The reason for this difference in $|\mathbf{G_{MEP}}|$ between this study and Slama's is not clear, especially since both were conducted in the same laboratory with the same type of sensor. One potential reason is a systematic error in pressure sensor sensitivity in some sensors that caused the sensitivity *in vivo* to be lower than in the room-temperature calibration vial. This potential source of error affects only the basic sensitivity of the sensor, not its frequency response (see Sec. 2.3).

At high frequencies, $\mathbf{G_{MEP}}$ from the various studies diverges. $|\mathbf{G_{MEP}}|$ decreases more rapidly and $\angle\mathbf{G_{MEP}}$ is flatter above 12 kHz in the Décory study (Décory, 1989; Décory et al., 1990) than in this one. Décory et al. (1990) consider sensor location as a possible source of error: in that study, the $\mathbf{P_{SV}}$ sensor was located about 5.5 mm from the OW, which is near the best place for a 5-kHz signal, and they suggest that $\mathbf{P_{SV}}$ at higher frequencies (shown dashed) could be affected by sound pressure from a cochlear traveling wave. In the Slama study (Slama, 2008; Slama et al., 2009, in press), $|\mathbf{G_{MEP}}|$ is considerably higher near 5 kHz and lower above 12 kHz than in this study, and $\angle\mathbf{G_{MEP}}$ accumulates more rapidly to 15 kHz and then reverses. The location of the TM sound pressure microphone was further from the TM in the Slama study than in this one, and the $\mathbf{G_{MEP}}$ differences above 12 kHz mentioned above are consistent with differences in sound pressure between the microphone location and the TM due to standing waves in the ear canal (see e.g., Dong and Olson, 2006; Ravicz et al., 2007).

Our measurements of $\mathbf{G_{MEP}}$ exhibit several similarities to $\mathbf{G_{MEP}}$ in other mammalian species but also some differences. Figure 7 compares our mean $\mathbf{G_{MEP}}$ to $\mathbf{G_{MEP}}$ in gerbil (Olson, 2001; fiber-optic pressure sensor), guinea pig (Décory et al., 1990; hydrophone and probe tube), cat (Nedzelnitsky, 1980; hydrophone and probe tube), and human temporal bones (Nakajima

et al., 2009; fiber-optic pressure sensor). In all species shown, $|\mathbf{G_{MEP}}|$ shows a plateau (where $|\mathbf{G_{MEP}}|$ is approximately constant over a wide frequency range), and $\angle\mathbf{G_{MEP}}$ is >0 at low frequencies and accumulates as frequency increases. Our chinchilla $|\mathbf{G_{MEP}}|$ is higher below 300 Hz than in the other species and higher above 12 kHz than in other species except gerbil, consistent with the relative stapes velocity transfer functions among these species (Rosowski, 1994). Another difference is that $\angle\mathbf{G_{MEP}}$ in chinchilla goes to 0 more abruptly and at a lower frequency (300 Hz) than $\angle\mathbf{G_{MEP}}$ in the other species (700 Hz – 2 kHz).

Above the upper plateau frequency, $|\mathbf{G_{MEP}}|$ decreases rapidly with frequency to 0 dB or below in all species measured (except for gerbil[2]). This upper plateau frequency marks the upper frequency limit of effective middle-ear transmission and so could be expected to set the upper limit of hearing ability (e.g., Rosowski, 1991). If so, extending $|\mathbf{G_{MEP}}|$ measurements in gerbil (which has a higher upper frequency hearing limit than the other species listed here) to higher frequencies may show an upper plateau frequency as well.

As noted by Puria et al. (1997), the maximum $|\mathbf{G_{MEP}}|$ (near 1 kHz) in several mammalian species is generally 6 dB or so below the "anatomical transformer ratio" computed as the product of the "ossicular lever ratio" (length of the manubrium of the malleus to incus long process) and the "area ratio" (area of TM to stapes footplate). Our $|\mathbf{G_{MEP}}|$ is generally about 10 dB below the chinchilla transformer ratio of 35 dB computed from a lever ratio of 6 dB (Fleischer, 1973) and an area ratio of 29 dB (Vrettakos et al., 1988). This result that $|\mathbf{G_{MEP}}|$ is less than the transformer ratio is reasonable: (a) the flexibility observed in the ossicular chain of several mammals can reduce middle-ear transmission at low and medium frequencies (e.g., Guinan and Peake, 1965; Nakajima et al., 2005), and (b) the very compliant chinchilla TM (e.g., Rosowski et al., 2006) does not move as a unit at frequencies above a few hundred Hz (Rosowski et al., 2009), so the effective TM area that influences middle-ear transmission may be smaller than the anatomical area.

4.6 Comparison of $\Delta\mathbf{P_{CP}}$ with other studies

The relationship of $\Delta\mathbf{P_{CP}}$ among species in which $\Delta\mathbf{P_{CP}}$ data from simultaneous measurements have been published is shown in Figure 8: chinchilla (this study), cat (Nedzelnitsky, 1980), and human (Nakajima et al., 2009). Also included in Fig. 8 are $\Delta\mathbf{P_{CP}}$ estimates computed from $\mathbf{P_{SV}}$ and $\mathbf{P_{ST}}$ that were measured in the same study but not necessarily in the same individuals: gerbil (Olson, 2001) and chinchilla and guinea pig (Décory et al., 1990). (The Décory chinchilla data are shown dashed below 0.5 kHz where they are estimated from $\mathbf{G_{MEP}}$ and above 5 kHz as discussed in Sec. 4.5.) The relationship between $\Delta\mathbf{P_{CP}}$ among these species is generally similar to the relationship of $\mathbf{G_{MEP}}$ (see Fig. 7): $|\Delta\mathbf{P_{CP}}|$ is approximately constant across a wide frequency range, and our chinchilla $|\Delta\mathbf{P_{CP}}|$ is generally lower than $|\Delta\mathbf{P_{CP}}|$ in other species between 300 Hz and 20 kHz (except human) and generally higher at low and high frequencies. Our chinchilla $|\Delta\mathbf{P_{CP}}|$ and $|\Delta\mathbf{P_{CP}}|$ in human show a high-frequency rolloff and are less than 0 dB at high frequencies (21 kHz or 10 kHz respectively); $|\Delta\mathbf{P_{CP}}|$ in other species remains above 0 dB at the highest frequencies that $\mathbf{P_{ST}}$ was measured (58 kHz for gerbil, 20 kHz for Décory chinchilla and guinea pig, 6 kHz for cat). $\angle\Delta\mathbf{P_{CP}}$ in all species shows a phase accumulation characteristic of a delay, but $\angle\Delta\mathbf{P_{CP}}$ accumulates much more rapidly in human than in the other species.

Similarly, the relationship between $\Delta\mathbf{P_{CP}}$ and $\mathbf{G_{MEP}}$ (see Fig. 7) is generally similar among these species. $|\Delta\mathbf{P_{CP}}|$ is nearly identical to $|\mathbf{G_{MEP}}|$ at low and middle frequencies and lower than $|\mathbf{G_{MEP}}|$ by only a few dB at high frequencies. $\angle\Delta\mathbf{P_{CP}}$ is similar to $\angle\mathbf{G_{MEP}}$ at low

[2]In other $\mathbf{G_{MEP}}$ studies in gerbil, in which ear canal sound pressure was measured further from the TM, an upper plateau frequency was seen near 40 kHz (Dong and Olson, 2006).

frequencies but has a greater accumulation above a few kHz. In general, except for slightly greater phase accumulation at high frequencies, $\mathbf{G_{MEP}}$ is a good approximation of $\Delta\mathbf{P_{CP}}$ in all species measured.

As mentioned above, $|\Delta\mathbf{P_{CP}}|$ in two species (chinchilla and human) has been shown to be bandpass with a high-frequency as well as a low-frequency limit. In these species, $|\Delta\mathbf{P_{CP}}|$ decreases to 0 dB (no middle-ear pressure gain) at a frequency near the upper audiometric limit. This result supports the idea that the frequency limits of hearing are strongly influenced by the limits of middle-ear function. It remains to be seen whether higher-frequency $\Delta\mathbf{P_{CP}}$ data in other species will also support this idea.

4.7 Input impedance of the cochlear partition

The cochlear input impedance $\mathbf{Z_C}$, the ratio of $\mathbf{P_{SV}}$ to stapes volume velocity, is a measure of power absorption in the cochlea. We use our calculations of the trans-cochlear-partition differential pressure and previous measurements of $\mathbf{Z_C}$ to estimate the input impedance of the cochlear partition $\mathbf{Z_{CP}}$, which can provide an indication of the power absorbed by the cochlear partition itself. $\mathbf{Z_{CP}}$ is different from the local (pointwise) cochlear partition impedance (see C_{CP} in the model in Fig. 4 and the Appendix); on the contrary, $\mathbf{Z_{CP}}$ is the distributed cochlear partition impedance (the integral of the local cochlear partition impedance and the mass of the scalae fluids at all points along the length of the cochlea) seen from the OW.3

The model of Figure 4 suggests that $\mathbf{Z_{CP}}$ is the primary determinant of $\Delta\mathbf{P_{CP}}$, at least at frequencies below about 10 kHz; therefore, $\mathbf{Z_{CP}}$ can be computed from $\mathbf{Z_C}$ by considering $\mathbf{Z_C}$ to be the series combination of $\mathbf{Z_{CP}}$ and the impedance of other cochlear structures (including the round window). In this case, $\mathbf{Z_{CP}}$ and $\mathbf{ZC}$ form a pressure divider, where $\mathbf{P_{SV}}-\mathbf{P_{ST}}$ is the pressure drop across $\mathbf{Z_{CP}}$ and $\mathbf{P_{SV}}$ is the pressure drop across $\mathbf{Z_C}$. $\mathbf{Z_{CP}}$ is computed from $\mathbf{Z_C}$ by multiplying $\mathbf{Z_C}$ by the ratio of $\Delta\mathbf{P_{CP}}$ to $\mathbf{G_{MEP}}$:

$$\mathbf{Z_{CP}}=\mathbf{Z_C}\cdot\Delta\mathbf{P_{CP}}/\mathbf{G_{MEP}}. \quad (2)$$

An estimate of $\mathbf{Z_{CP}}$ computed from our $\mathbf{G_{MEP}}$, our $\Delta\mathbf{P_{CP}}$, and the $\mathbf{Z_C}$ presented by Slama et al. (Slama, 2008; Slama et al., in press, calculated from simultaneous measurements of $\mathbf{P_{SV}}$ and stapes velocity $\mathbf{V_S}$ and previously-published estimates of stapes footplate area) is shown in Figure 9. $\mathbf{Z_{CP}}$ is more resistive than $\mathbf{Z_C}$, as is shown by the flatter $|\mathbf{Z_{CP}}|$ with frequency and the $\angle\mathbf{Z_{CP}}$ closer to zero above 1 kHz. At low frequencies $\mathbf{Z_{CP}}$ is very similar to $\mathbf{Z_C}$, as in this frequency range $|\mathbf{P_{STn}}| \ll |\mathbf{G_{MEP}}|$ (Fig. 4) and $\Delta\mathbf{P_{CP}} \approx \mathbf{G_{MEP}}$. At high frequencies $\Delta\mathbf{P_{CP}} \neq \mathbf{G_{MEP}}$, and there is a more substantial difference between $\mathbf{Z_{CP}}$ and $\mathbf{Z_C}$. Above 20 kHz $|\mathbf{Z_{CP}}|$ increases somewhat; $\angle\mathbf{Z_{CP}}$ decreases dramatically to less than −0.25 cycles, which implies that energy is introduced into the system. This could be real, as the location of the scala tympani sensor (12-kHz place) is not far from the 20-kHz place. Alternatively, $\mathbf{P_{SV}}$ or $\mathbf{P_{ST}}$ at the measurement location could be significantly different from $\mathbf{P_{SV}}$ or $\mathbf{P_{ST}}$ at the cochlear base (e.g., Olson, 2001) or transverse stapes motion (e.g., Decraemer et al., 2007 in gerbil) could have influenced $\mathbf{V_S}$ measurements. Despite this possible shortcoming, this estimate of $\mathbf{Z_{CP}}$ provides important empirical data for cochlear modeling.

5. Summary and Conclusions

(1) Middle-ear pressure gain $\mathbf{G_{MEP}}$ has approximately constant magnitude (~20 dB) over a wide frequency range (0.3 to 20 kHz) and includes a delay of about 40 μsec, comparable to the delay between stapes velocity and ear canal sound pressure. $|\mathbf{G_{MEP}}|$ decreases rapidly with frequency to 0 dB (unity gain) at 20 kHz.

(2) The trans-cochlear-partition sound pressure $\Delta\mathbf{P_{CP}}$, which represents the effective input to the cochlea, is governed by $\mathbf{G_{MEP}}$ below 5 kHz but is influenced by scala tympani pressure $\mathbf{P_{STn}}$ at higher frequencies.

(3) The magnitude of $\Delta\mathbf{P_{CP}}$ is also approximately constant between 300 Hz and 20 kHz and decreases sharply at higher frequencies. The frequency of the sharp decrease is similar to the high-frequency limit of the chinchilla audiogram.

(4) The input impedance of the cochlear partition $\mathbf{Z_{CP}}$, which is an indicator of power absorption by the cochlear partition, is resistive from 300 Hz to about 20 kHz.

The work described here extends the applicability of the chinchilla as a model for studying not only the effects of middle- and inner-ear pathologies on middle- and inner-ear mechanics but also nonacoustic stimulation of the inner ear. $\Delta\mathbf{P_{CP}}$ provides an assay of cochlear response to "bone conduction" stimuli (delivered through a vibrator attached to the skull) to study the mechanisms of sound transmission to the physiologically active cochlea through the intact head. This more direct measure of cochlea response is useful for testing hypotheses of the relative importance of different bone conduction modes (e.g., Khanna et al., 1976; Stenfelt and Goode, 2005) in normal ears and in ears with inner-ear pathology such as superior semicircular canal dehiscence syndrome (SCD syndrome – Songer, 2006). These measurements also add to the knowledge of chinchilla middle-ear mechanics and, in concert with previous measurements of other middle-ear properties, provide a more complete view of middle-ear function in this species. More complete knowledge of the entire auditory periphery makes the chinchilla preparation a more useful model for exploring middle- and inner-ear function.

Acknowledgments

We thank Elizabeth Olson and Wei Dong for much help in learning to fabricate and use the pressure sensors, Elizabeth Olson for sharing data, Melissa Wood for animal surgery, Heidi Nakajima for technical advice, and the staff of the Eaton-Peabody Laboratory for technical support. This work was carried out in part through the use of MIT's Microsystems Technology Laboratories and the help of Kurt Broderick and in part at the Center for Nanoscale Systems (CNS) with the help of Ed Macomber. CNS is a member of the National Nanotechnology Infrastructure Network (NNIN), which is supported by the National Science Foundation under NSF award no. ECS-0335765, and a part of the Faculty of Arts and Sciences at Harvard University. Supported by NIDCD.

Appendix: Formulation of a lumped-element cochlear model

The model of cochlear macromechanics presented in Fig. 4 is based approximately on a lumped-element model presented in Fig. 4 of Olson (2001). Unlike in Olson (2001), $\mathbf{P_{SV}}$ and $\mathbf{P_{ST}}$ were measured at different distances from the cochlear base and the round window was left intact for $\mathbf{P_{ST}}$ measurements, so the intervening fluid and the RW must be taken into account. The acoustic mass terms include not only the mass of the cochlear fluid between the sensor tip and the cochlear partition but also the mass of SV fluid between the stapes footplate and the $\mathbf{P_{ST}}$ measurement location and the mass of ST fluid between the $\mathbf{P_{ST}}$ measurement location and the RW. M_{SV} = acoustic mass of SV fluid (perilymph and endolymph) between the apical edge of the stapes footplate and the location of $\mathbf{P_{ST}}$ measurements; C_{CP} = local compliance of cochlear partition; R_{CP} = characteristic (transmission-line) resistance of the cochlea apical to the $\mathbf{P_{ST}}$ measurement location. We neglect the helicotrema; including a helicotrema impedance as described in Dallos, 1970 (computed from Dallos's value for chinchilla helicotrema radius) does not match low-frequency $\mathbf{P_{ST}}$ / $\mathbf{P_{SV}}$ estimates. $M_{\mathbf{ST}}$ = acoustic mass of ST perilymph; the arrow indicates that some of this ST mass can be between the $\mathbf{P_{ST}}$ sensor tip and the cochlear partition. In fact, we obtained the best model fit by putting all of the ST mass between the $\mathbf{P_{ST}}$ sensor and the RW. C_{RW} = round window compliance. Element values are based on previously-published physiological and anatomical measurements and adjusted slightly (and a resistance R_{RW}, not shown in Fig. 4, added in series with C_{RW}) to

match the data of Fig. 4. The radiation impedance from the round window Z_{RAD} is negligible and so is not included in Fig. 4. Element values and their sources and derivations are listed in Table A1.

Table A1

Element values and sources for lumped-element model of Figure 4.

Symbol	Element	Source or derivation	Value	Units
M_{SV}	SV mass	$\rho\, l_{SV} / S_{SV}$ Beranek, 1986, Eq. 5.42		kg / m^4
ρ	Fluid density	Assumed equal to water	1000	kg / m^3
l_{SV}	Distance from stapes to $\mathbf{P_{ST}}$ meas. location		1.7	mm
S_{SV}	SV cross-section area	Dallos, 1970, Fig. 10; adjusted to fit data	1.0	mm^2
C_{CP}	Local CP compliance	$w_{bm}\, l_{bm} / k_{CP}$ Olson, 2001	4×10^{-16}	m^3 / Pa
w_{bm}	Basilar membrane width	Dallos, 1970, Fig. 10; adjusted per Ruggero et al., 1990	0.13	mm
l_{bm}	Effective basilar membrane length	Olson, 2001; adjusted to fit data	0.3	mm
k_{CP}	Local CP mechanical stiffness	Ruggero et al., 1997; de La Rochefoucauld and Olson, 2007	0.7	Pa / nm
R_{CP}	Cochlear resistance	Computed from Slama, 2008	9×10^{10}	mks Ω
M_{ST}	ST mass	$\rho\, l_{ST} / S_{ST}$ Beranek, 1986, Eq. 5.42		kg / m^4
l_{ST}	Distance from $\mathbf{P_{ST}}$ meas. location to RW		1.0	mm
S_{ST}	ST cross-section area	Estimated from S_{SV} per Ruggero et al., 1990; adjusted to fit data	0.5	mm^2
C_{RW}	RW compliance	Lynch et al., 1982 (for cat)	1×10^{-13}	m^3 / Pa
R_{RW}	RW resistance	To fit data 300–400 Hz	2×10^9	mks Ω
Z_{RAD}	Radiation impedance of RW	Beranek, 1986, Table 5.1 for a = 0.34 mm	$< 10^6$	mks Ω

Abbreviations

C_{CP}	model local compliance of cochlear partition
CP	cochlear potential
C_{RW}	model local compliance of round window
f	frequency
G_{MEP}	middle-ear pressure gain
M_{ST}	model mass of scala tympani fluid
M_{SV}	model mass of scala vestibuli fluid
OW	oval window
$\Delta\mathbf{P_{CP}}$	normalized differential trans-cochlear-partition pressure
P_{EC}	sound pressure in the ear canal relatively far from the tympanic membrane
P_{ST}	scala tympani sound pressure
P_{STn}	scala tympani sound pressure normalized by sound pressure near the tympanic membrane

P_{SV}	scala vestibuli sound pressure
P_{TM}	sound pressure in the ear canal near the tympanic membrane
P_0	sound pressure in calibration setup
R_{CP}	model cumulative resistance of cochlear partition
RW	round window
TM	tympanic membrane
V_S	velocity of a point on the stapes
v_{sens}	pressure sensor output voltage
Z_C	cochlear input impedance
Z_{CP}	input impedance of the cochlear partition as seen from the vestibule

References

Beranek, LL. Acoustics. Acoustical Society of America; Melville, NY: 1986.

Dallos P. Low-frequency auditory characteristics: Species dependence. J. Acoust. Soc. Am 1970;48:489–499. [PubMed: 5470495]

Dancer A, Franke R. Intracochlear sound pressure measurements in guinea pigs. Hear. Res 1980;2:191–205. [PubMed: 7410227]

Décory, L. Origine des différences interspécifiques de susceptibilités au bruit. Thèse de Doctorat de l'Université de Bordeaux; France: 1989.

Décory, L.; Franke, RB.; Dancer, AL. Measurement of the middle ear transfer function in cat, chinchilla and guinea pig. In: Dallos, P.; Geisler, CD.; Matthews, JW.; Ruggero, MA.; Steele, CR., editors. The Mechanics and Biophysics of Hearing. Springer; Berlin: 1990. p. 270-277.

Decraemer WF, de La Rochefoucauld O, Dong W, Khanna SM, Olson ES. Scala vestibuli pressure and three-dimensional stapes velocity measured in direct succession in gerbil. J. Acoust. Soc. Am 2007;121:2774–2791. [PubMed: 17550177]

Dong W, Olson ES. Middle ear forward and reverse transmission in gerbil. J. Neurophysiol 2006;95:2951–2961. [PubMed: 16481455]

Drescher DG, Eldredge DH. Species differences in cochlear fatigue related to acoustics of outer and middle ears of guinea pig and chinchilla. J. Acoust. Soc. Am 1974;56:929–934. [PubMed: 4421145]

Eldridge DH, Miller JD, Bohne BA. A frequency-position map for the chinchilla cochlea. J. Acoust. Soc. Am 1981;69:1091–1095. [PubMed: 7229195]

Fleischer G. Studien am Skelett des Gehörorgans der Säugetiere, einschliesslich des Menschen. Säugetierkundl Mitteilungen (München) 1973;21:131–239.

Guinan JJ, Peake WT. Middle-ear characteristics of anesthetized cats. J. Acoust. Soc. Am 1965;41:1237–1261. [PubMed: 6074788]

Khanna SM, Tonndorf J, Queller JE. Mechanical parameters of hearing by bone conduction. J. Acoust. Soc. Am 1976;60:139–154. [PubMed: 956521]

de La Rochefoucauld O, Olson ES. The role of Organ of Corti mass in passive cochlear tuning. Biophys. J 2007;93:3434–3450. [PubMed: 17905841]

Lynch TJ III, Nedzelnitsky V, Peake WT. Input impedance of the cochlea in cat. J. Acoust. Soc. Am 1982;72:108–130. [PubMed: 7108034]

Nakajima HH, Dong W, Olson ES, Merchant SN, Ravicz ME, Rosowski JJ. Differential intracochlear sound pressure measurements in normal human temporal bones. J. Assoc. Res. Otolaryngol 2009;10:23–36. [PubMed: 19067078]

Nakajima HH, Ravicz ME, Merchant SN, Peake WT, Rosowski JJ. Experimental ossicular fixations and the middle ear's response to sound: Evidence for a flexible ossicular chain. Hear. Res 2005;204:60–77. [PubMed: 15925192]

Nedzelnitsky V. Sound pressure in the basal turn of the cat cochlea. J. Acoust. Soc. Am 1980;68:1676–1689. [PubMed: 7462467]

Olson ES. Observing middle and inner ear mechanics with novel intracochlear pressure sensors. J. Acoust. Soc. Am 1998;103:3445–3463. [PubMed: 9637031]

Olson ES. Intracochlear pressure measurements related to cochlear tuning. J. Acoust. Soc. Am 2001;110:349–367. [PubMed: 11508960]

Peake WT, Rosowski JJ, Lynch TJ III. Middle-ear transmission: Acoustic versus ossicular coupling in cat and human. Hear. Res 1992;57:245–268. [PubMed: 1733916]

Puria S, Peake WT, Rosowski JJ. Sound-pressure measurements in the cochlear vestibule of human-cadaver ears. J. Acoust. Soc. Am 1997;101:2754–2770. [PubMed: 9165730]

Ravicz ME, Olson ES, Rosowski JJ. Sound pressure distribution and power flow within the gerbil ear canal from 100 Hz to 80 kHz. J. Acoust. Soc. Am 2007;122:2154–2173. [PubMed: 17902852]

Rosowski JJ. The effects of external and middle ear filtering on auditory threshold and noise-induced hearing loss. J. Acoust. Soc. Am 1991;90:124–135. [PubMed: 1880280]

Rosowski, JJ. Outer and middle ear. In: Fay, RR.; Popper, AN., editors. Comparative Hearing in Mammals. Springer-Verlag; New York: 1994. p. 172-247.

Rosowski JJ, Cheng JT, Ravicz ME, Hulli N, Hernandez-Montes M, Harrington E, Furlong C. Computer-assisted time-averaged holograms of the surface of the mammalian tympanic membrane with sound stimuli of 0.4–25 kHz. Hearing Research 2009;253:83–96. [PubMed: 19328841]

Rosowski JJ, Ravicz ME, Songer JE. Structures that contribute to middle-ear admittance in chinchilla. J. Comp. Physiol. A 2006;192:1287–1311.

Ruggero MA, Rich NC, Recio A, Narayan SS, Robles L. Basilar-membrane responses to tones at the base of the chinchilla cochlea. J. Acoust. Soc. Am 1997;101:2151–2163. [PubMed: 9104018]

Ruggero MA, Rich NC, Robles L, Shivapuja BG. Middle-ear response in the chinchilla and its relationship to mechanics at the base of the cochlea. J. Acoust. Soc. Am 1990;87:1612–1629. [PubMed: 2341666]

Schloss F, Strasberg M. Hydrophone calibration in a vibrating column of liquid. J. Acoust. Soc. Am 1962;34:958–960.

Shera CA, Zweig G. Middle-ear phenomenology: The view from the three windows. J. Acoust. Soc. Am 1992;92:1356–1370. [PubMed: 1401522]

Slama, MCC. M.S. thesis. Massachusetts Institute of Technology; Cambridge, MA: 2008. Middle ear pressure gain and cochlear input impedance in the chinchilla.

Slama, MCC.; Ravicz, ME.; Nakajima, HH.; Dong, W.; Rosowski, JJ. Measurements of middle ear pressure gain and cochlear input impedance in the chinchilla. In: Cooper, NP.; Kemp, DT., editors. Concepts and Challenges in the Biophysics of Hearing. World Scientific; New Jersey: 2009. p. 9-14.

Slama MCC, Ravicz ME, Rosowski JJ. Middle ear function and cochlear input impedance in chinchilla. J. Acoust. Soc. Am. in press.

Songer, JE. Ph.D. thesis. Massachusetts Institute of Technology; Cambridge, MA: 2006. Superior Canal Dehiscence: Auditory Mechanisms.

Songer JE, Rosowski JJ. The effect of superior-canal opening on middle ear input admittance and air-conducted stapes velocity in chinchilla. J. Acoust. Soc. Am 2006;120:258–269. [PubMed: 16875223]

Stenfelt S, Goode RL. Transmission properties of bone conducted sound: Measurements in cadaver heads. J. Acoust. Soc. Am 2005;118:2373–2391. [PubMed: 16266160]

Vrettakos PA, Dear SP, Saunders JC. Middle ear structure in the chinchilla: A quantitative study. Am. J. Otolaryngol 1988;9:58–67. [PubMed: 3400821]

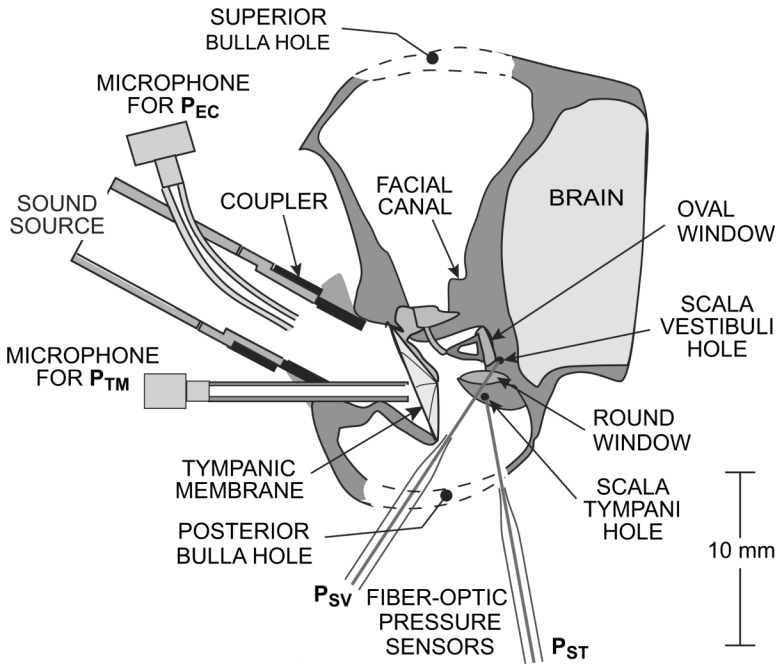

Figure 1.

Diagram of a chinchilla left ear showing the preparation and the placement of microphones and fiber-optic pressure sensors. An earphone (not shown) was connected to the sound source. Sound pressure in the ear canal was measured by probe-tube microphones near the source ($\mathbf{P_{EC}}$) and near the umbo within the TM ($\mathbf{P_{TM}}$). Sound pressure in the cochlear scalae was measured by pressure sensors inserted through small holes into scala vestibuli ($\mathbf{P_{SV}}$) and scala tympani ($\mathbf{P_{ST}}$).

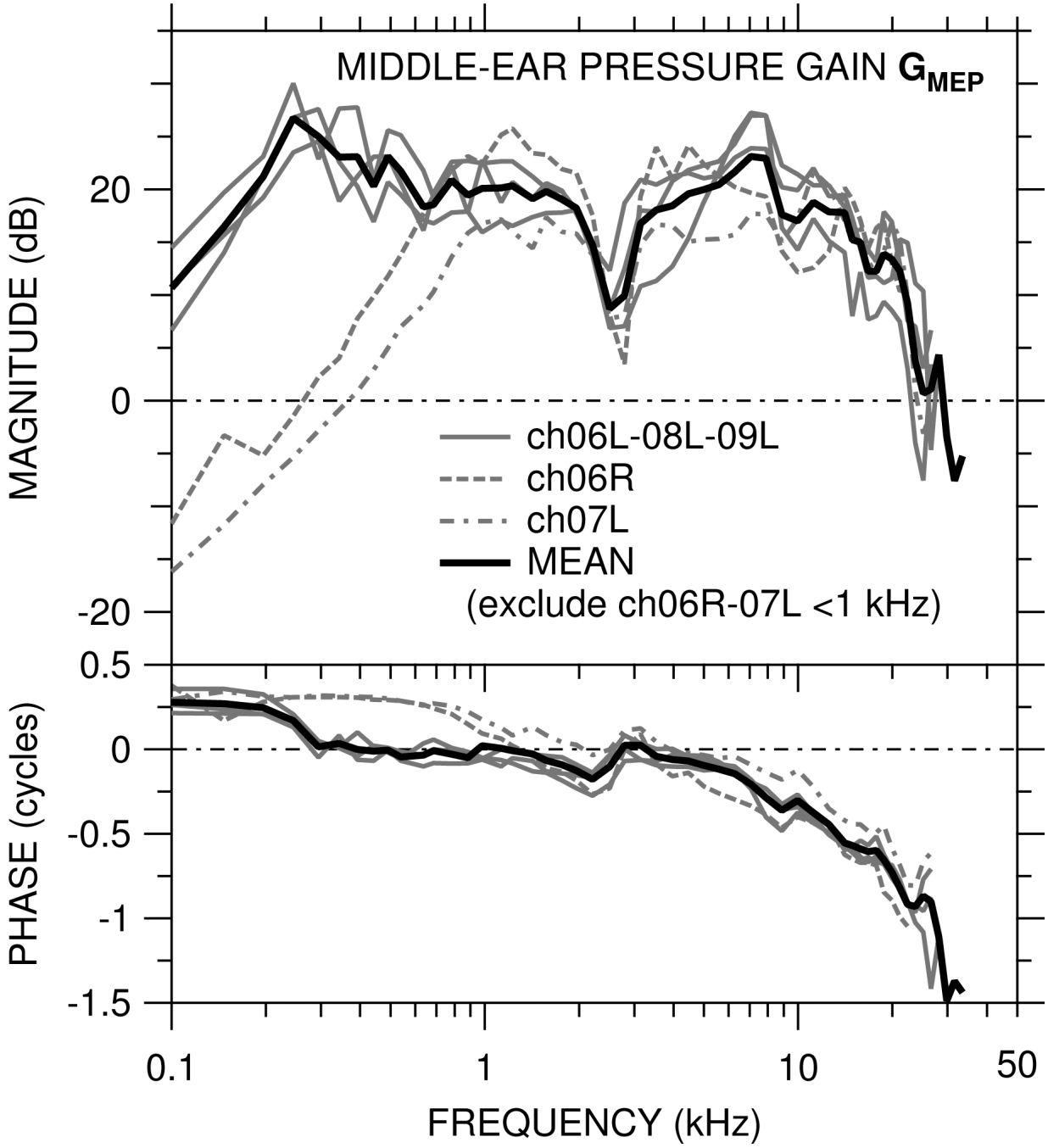

Figure 2.

Middle-ear pressure gain $\mathbf{G_{MEP}} = \mathbf{P_{SV}} / \mathbf{P_{TM}}$ in five ears. Top: magnitude $|\mathbf{G_{MEP}}|$ in dB; bottom: phase $\angle\mathbf{G_{MEP}}$ in cycles. In two ears (ch06R, ch07L) the bone near the OW was cracked while the scala vestibuli hole was drilled. $\mathbf{G_{MEP}}$ in those ears (dashed, dot-dashed lines) is included in the logarithmic mean (solid black line) only at 1 kHz and above.

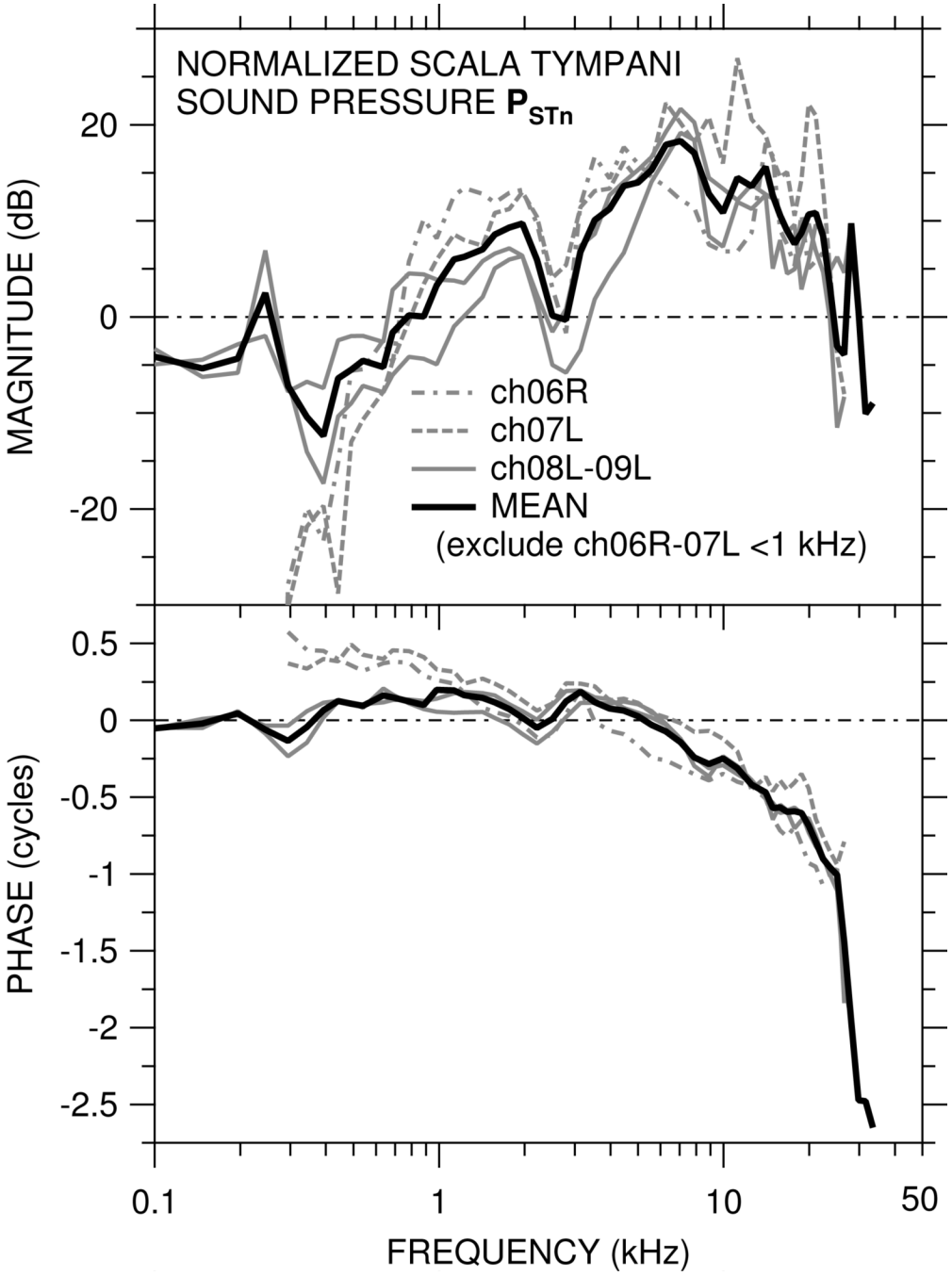

Figure 3.

Scala tympani sound pressure $\mathbf{P_{STn}} = \mathbf{P_{ST}} / \mathbf{P_{TM}}$ in four ears. Top: magnitude in dB; bottom: phase in cycles. In the two ears (ch06R, ch07L) in which the bone near the OW was cracked, $\mathbf{P_{STn}}$ (dashed, dot-dashed lines) is included in the logarithmic mean (solid black line) only at 1 kHz and above, and data are omitted below 300 Hz where $|\mathbf{P_{STn}}|$ was at the noise floor.

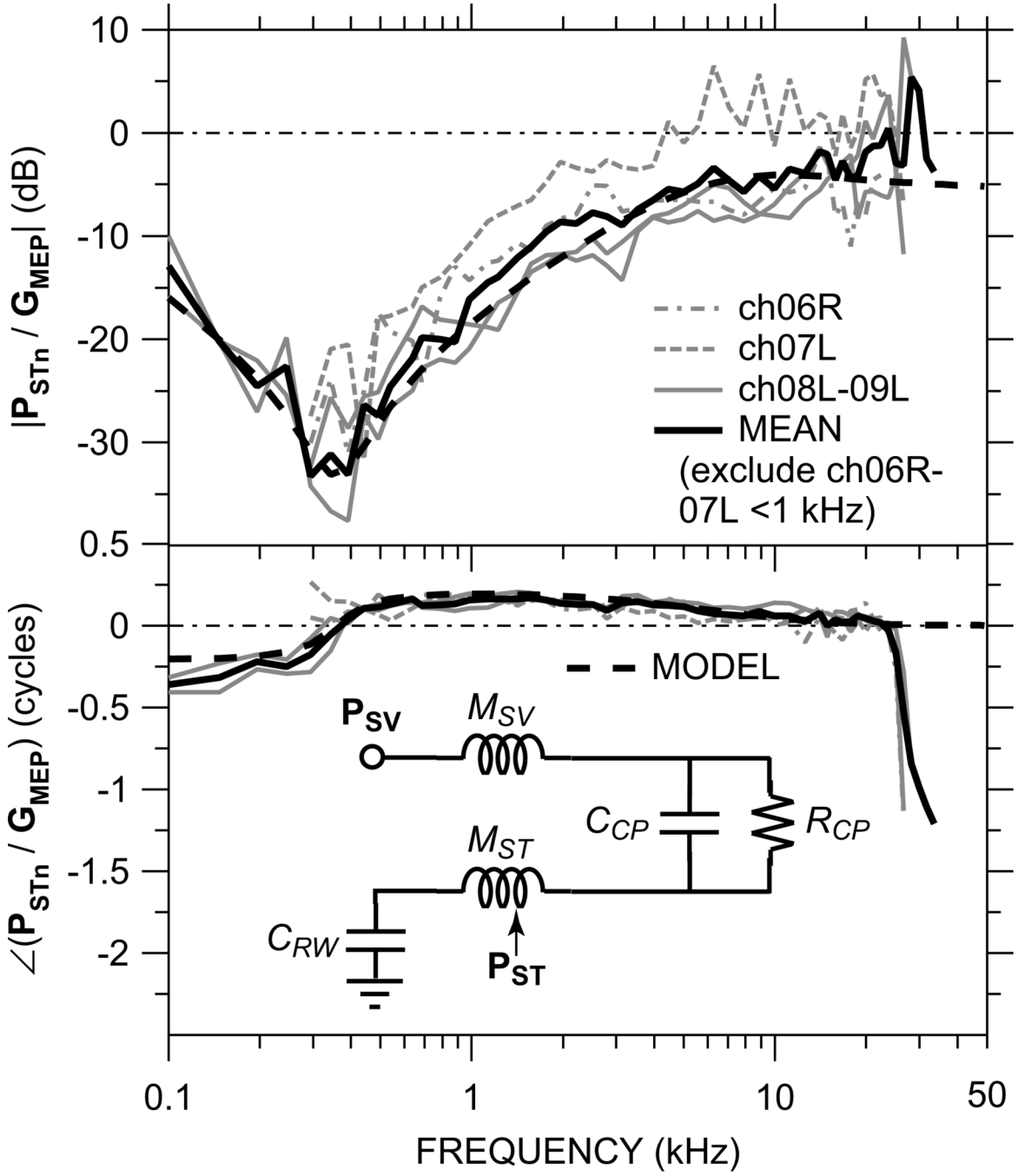

Figure 4.

The ratio of $\mathbf{P_{STn}}$ to $\mathbf{G_{MEP}}$ (equivalent to $\mathbf{P_{ST}}$ / $\mathbf{P_{SV}}$ for the same $\mathbf{P_{TM}}$) in each of the four ears in which both $\mathbf{P_{SV}}$ and $\mathbf{P_{ST}}$ were measured. Top: magnitude in dB; bottom: phase in cycles. In the two ears in which the bone near the OW was cracked (ch06R, ch07L – dashed, dot-dashed gray lines), data are omitted below 300 Hz and included in the logarithmic mean (solid black line) only at 1 kHz and above. Inset in bottom panel: Simple lumped-element circuit model of cochlear macromechanics to predict $\mathbf{P_{ST}}$ / $\mathbf{P_{SV}}$ (dashed black line).

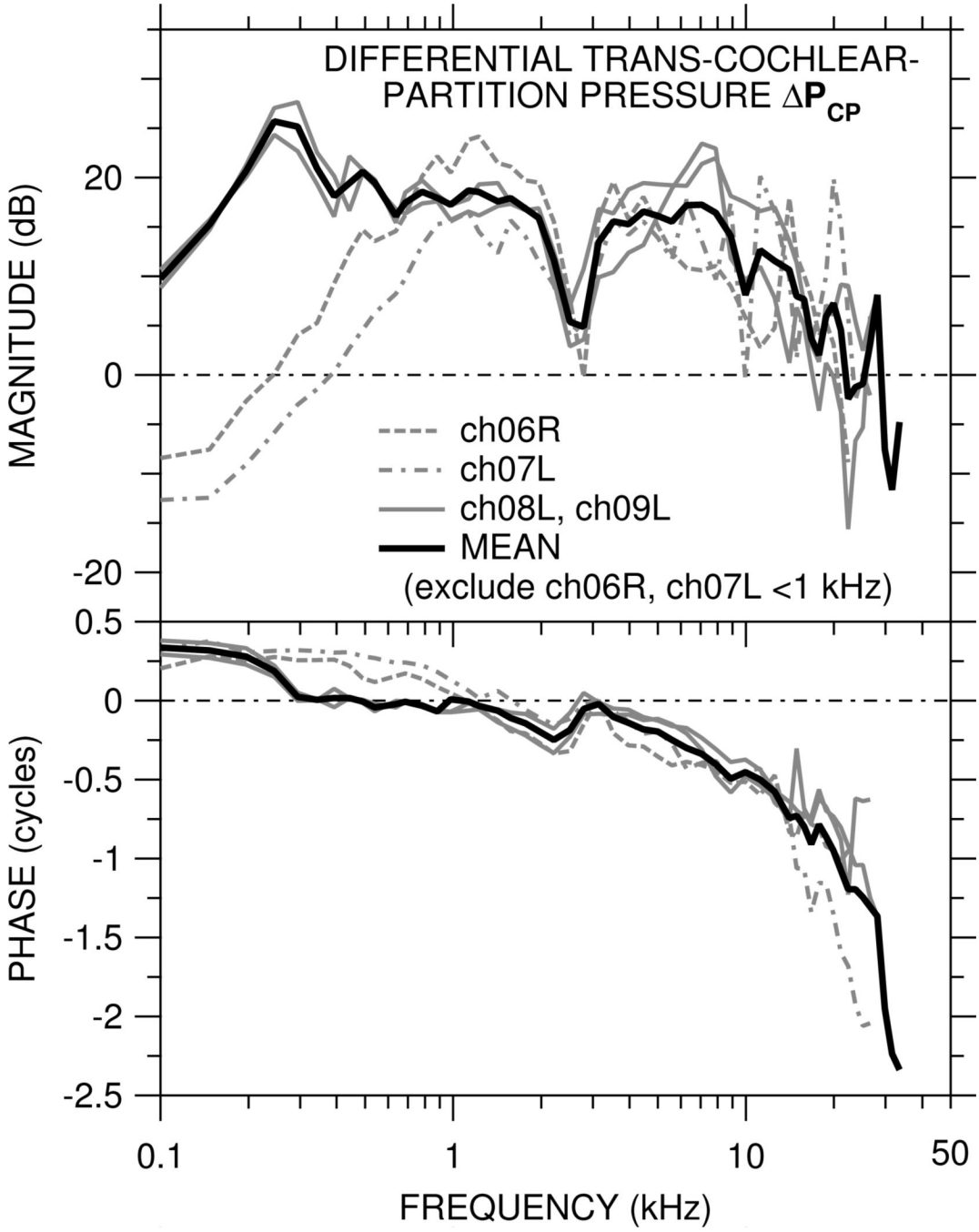

Figure 5.

Differential trans-cochlear-partition pressure $\Delta\mathbf{P_{CP}} = \mathbf{G_{MEP}}-\mathbf{P_{STn}}$ in each of the four ears in which both $\mathbf{P_{SV}}$ and $\mathbf{P_{ST}}$ were measured. Top: magnitude in dB; bottom: phase in cycles. In the two ears (ch06R, ch07L) in which the bone near the OW was cracked, $\Delta\mathbf{P_{CP}}$ (dashed, dot-dashed lines) is included in the logarithmic mean (solid black line) only at 1 kHz and above.

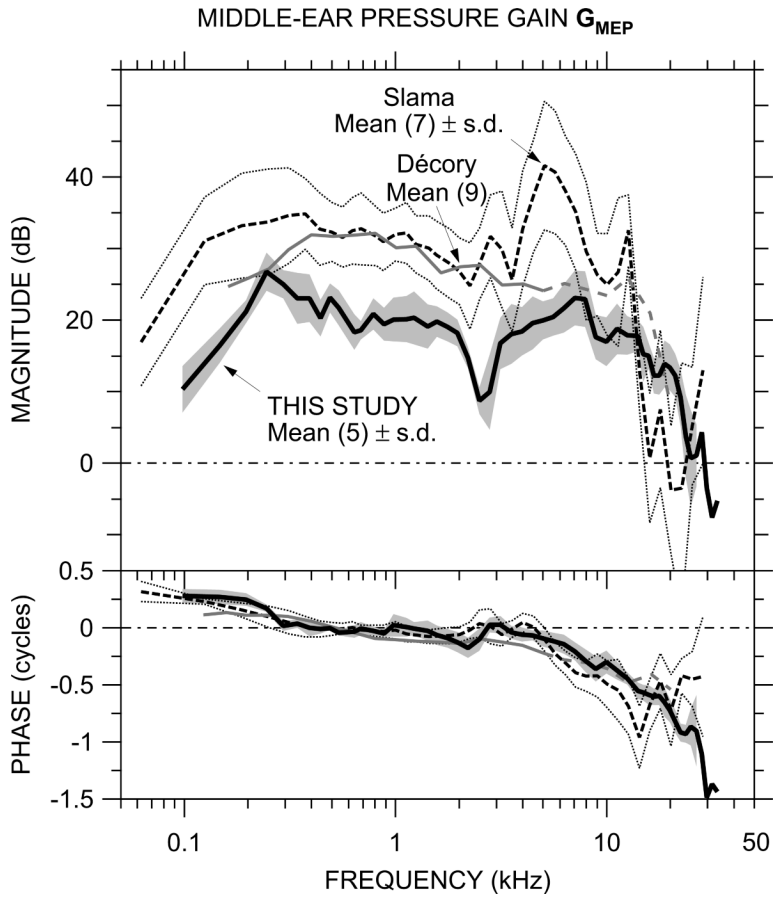

Figure 6.

Comparison of the mean $\mathbf{G_{MEP}}$ in this study (N=5, thick black line) to the mean $\mathbf{G_{MEP}}$ from other studies in chinchilla: Slama (2008, Slama et al. 2009; N=7, dashed line) and Décory (1989, Décory et al., 1990; N=9, thin gray line). The shaded area shows ± 1 standard deviation (s.d.) of the logarithmic mean in this study; the thin dotted lines show ± 1 s.d. of the logarithmic mean of the Slama et al. study. Décory data are dashed above 5 kHz (see text).

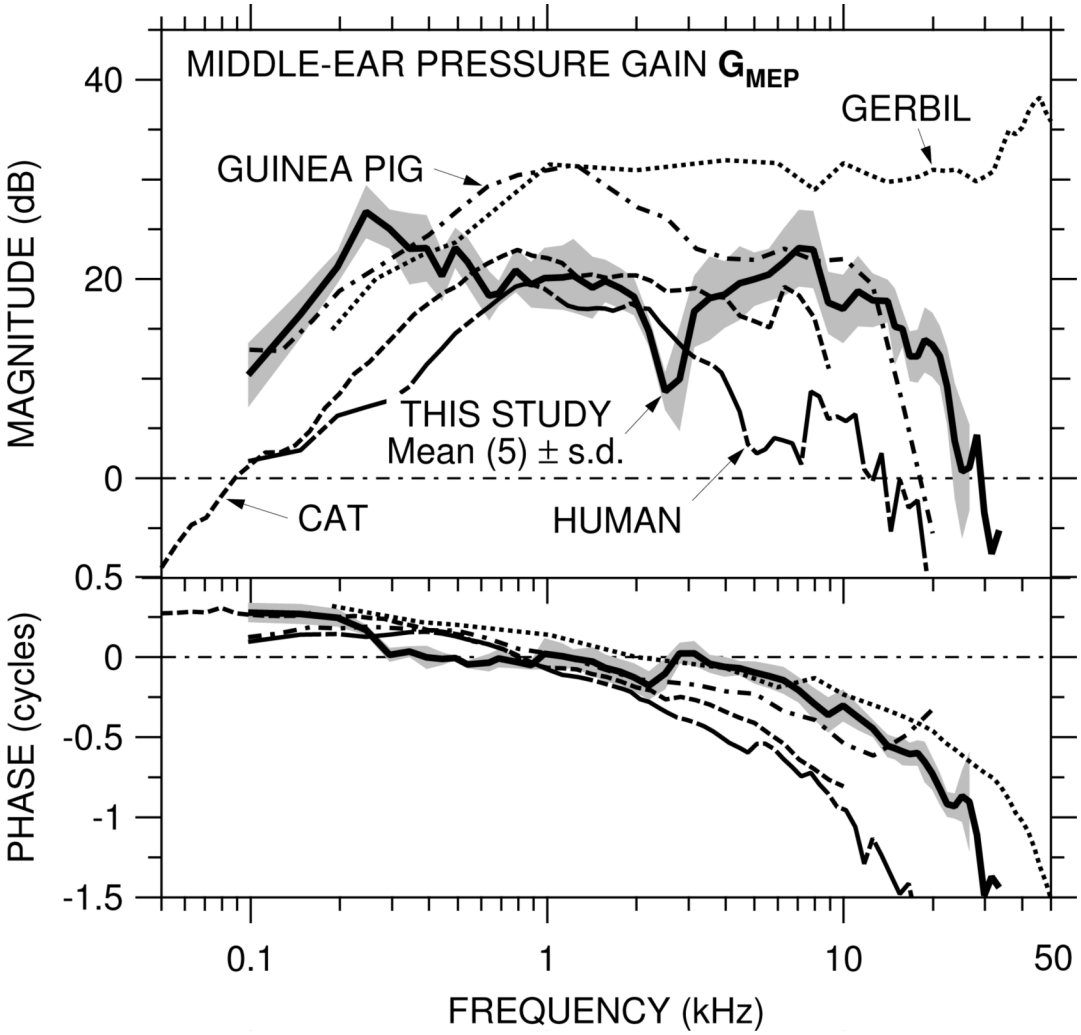

Figure 7.

Comparison of the mean $\mathbf{G_{MEP}}$ in this study (N=5; thick solid line) to the mean $\mathbf{G_{MEP}}$ from other studies in other species: gerbil (N=14; Olson, 2001; dotted line), guinea pig (N=11; Décory et al., 1990; dot-dashed line), cat (N=25; Nedzelnitsky, 1980; dashed line) and human (temporal bones: N=6; Nakajima et al., 2009; long dot-dashed line). The shaded area shows ± 1 s.d. of the logarithmic mean in this study.

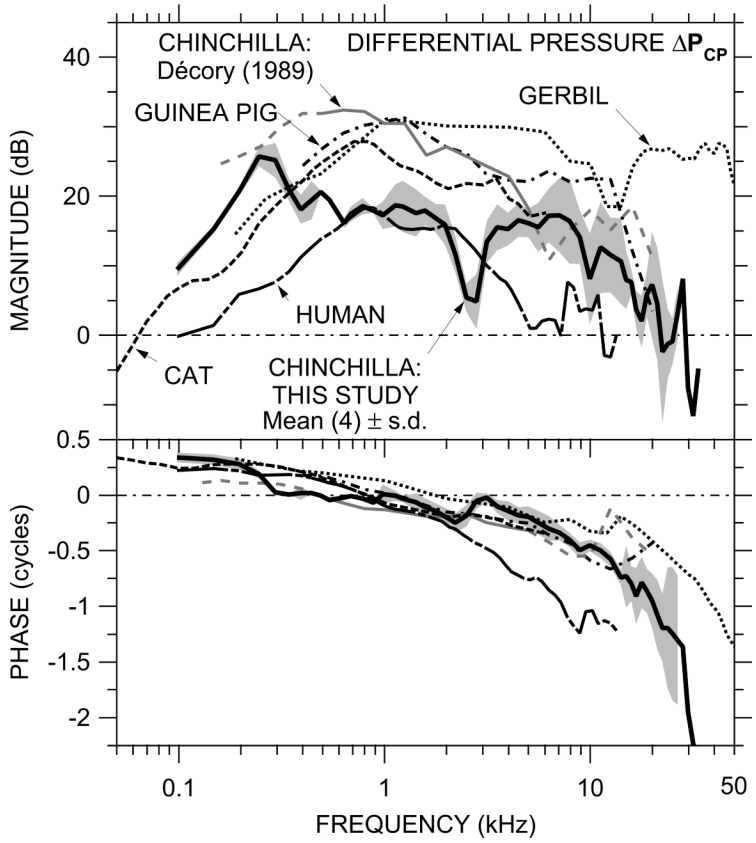

Figure 8.

Comparison of the mean $\Delta\mathbf{P}_{\mathbf{CP}}$ in this study (N=4; thick solid line) to published $\Delta\mathbf{P}_{\mathbf{CP}}$ in cat (median, N=6; Nedzelnitsky, 1980; dashed line) and human (temporal bones: N=6, Nakajima et al., 2009; long dot-dashed line) and $\Delta\mathbf{P}_{\mathbf{CP}}$ computed from $\mathbf{G}_{\mathbf{MEP}}$ and $\mathbf{P}_{\mathbf{STn}}$ in gerbil (N=14; Olson, 2001; dotted line), chinchilla (N=4; Décory et al., 1990; gray line solid or dashed <500 Hz and >5 kHz, see text), and guinea pig (Décory et al., 1990, N=5; dot-dashed line). The shaded area shows ± 1 s.d. of the logarithmic mean in this study.

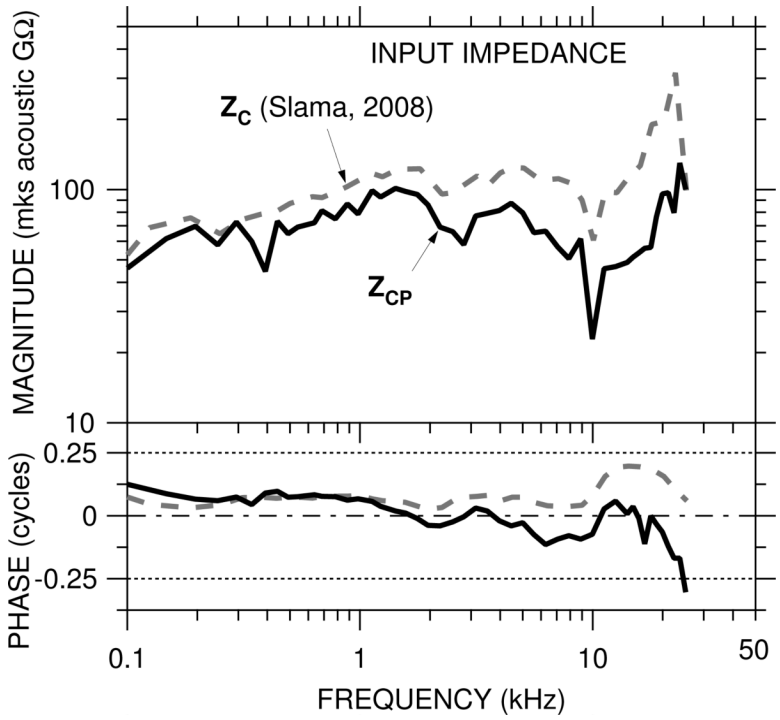

Figure 9.

Estimate of the overall impedance of the cochlear partition $\mathbf{Z_{CP}}$ (solid line), computed from $\mathbf{Z_C}$ (Slama, 2008, dashed line) and the ratio of $\Delta\mathbf{P_{CP}}$ to $\mathbf{G_{MEP}}$.